



Review

Recent advances in high temperature electrolysis using solid oxide fuel cells: A review

M.A. Laguna-Bercero*

Instituto de Ciencia de Materiales de Aragón, ICMA, CSIC – Universidad de Zaragoza, Pedro Cerbuna 12, 50009 Zaragoza, Spain

ARTICLE INFO

Article history:

Received 12 August 2011

Received in revised form

29 November 2011

Accepted 9 December 2011

Available online 9 January 2012

Keywords:

Solid oxide electrolysis cell

Hydrogen

High temperature electrolysis

Reversible SOFC

SOEC

Zirconia

ABSTRACT

New and more efficient energy conversion systems are required in the near future, due in part to the increase in oil prices and demand and also due to global warming. Fuel cells and hybrid systems present a promising future but in order to meet the demand, high amounts of hydrogen will be required. Until now, probably the cleanest method of producing hydrogen has been water electrolysis. In this field, solid oxide electrolysis cells (SOEC) have attracted a great interest in the last few years, as they offer significant power and higher efficiencies compared to conventional low temperature electrolyzers. Their applications, performances and material issues will be reviewed.

© 2011 Elsevier B.V. All rights reserved.

Contents

1. Introduction	5
1.1. History	5
1.2. Thermodynamics	5
1.3. Materials for solid oxide electrolysis cells	6
1.4. Proton conductor materials for high temperature steam electrolysis	6
2. Status of high temperature electrolysis using SOFC	6
2.1. Zirconia based SOEC	7
2.1.1. Yttria doped zirconia electrolytes	7
2.1.2. Scandia doped zirconia electrolytes	8
2.2. Ceria based electrolytes	8
2.3. LaGaO ₃ based electrolytes	8
2.4. Proton conducting electrolyte materials	9
2.5. Alternative designs for solid oxide electrolysis cells	10
2.6. Electrode materials for SOEC applications	11
2.6.1. Fuel electrodes for SOEC	11
2.6.2. Oxygen electrodes for SOEC	11
3. Materials degradation issues in solid oxide electrolysis cells	13
4. Modeling of solid oxide electrolysis cells and systems	14
5. Other applications using solid oxide electrolysis cells	15
6. Summary	15
Acknowledgements	15
References	15

* Tel.: +34 876 555152; fax: +34 976 761957.

E-mail address: malaguna@unizar.es

1. Introduction

Renewable energy resources have attracted great interest in recent years. A fundamental problem associated with renewable energy sources such as solar energy, wind power, hydropower or geothermal power is that they have to match supply with demand, and therefore energy storage is essential. Battery storage has been proposed as an alternative for some applications, although several problems such as high cost for large storage requirements, or loss of charge overtime are also associated. Energy storage in the form of hydrogen will also be essential and has been widely discussed for many years with an increasing drive toward the hydrogen economy. Hydrogen is probably the preferred energy carrier for a future zero-carbon economy but several research efforts are required in order to supply inexpensive and plentiful amounts of fuel. Although hydrogen is the most abundant element in nature, it is usually found as a compound combined with other elements, and thus, the production of hydrogen always requires energy. Current hydrogen production methods need the use of fossil fuels, such as steam reforming, partial oxidation of heavy hydrocarbons and gasification of coal. Other processes currently under development include reforming and pyrolysis using biomass and other carbon waste, direct methanol reforming, as well as fermentation of biomass and biological production. Moreover, there are also other hydrogen production methods that are generally categorized as electrochemical processes, including photoelectrochemical methods, thermochemical water splitting, and water electrolysis. Of these, only water electrolysis is currently commercially available. In addition, of all the methods to produce hydrogen, water electrolysis is probably the cleanest when combined with a renewable energy source to produce the electricity. Additional information regarding hydrogen production can be found in the following excellent reviews [1–19]. This review will focus on the production of hydrogen by high temperature electrolysis. Materials, performance and degradation issues of those devices will be reviewed in the manuscript.

1.1. History

Water electrolysis to produce hydrogen and oxygen gases is a well-known established process. Basically, the principle of a water electrolyser is to convert water and DC electricity into gaseous hydrogen and oxygen, that is to say the reverse of a hydrogen fuel cell. This process was firstly demonstrated by Nicholson and Carlisle in 1800. In the 1820s Faraday clarified the principles and in 1934 he introduced the word “electrolysis”. Electrolysis was not used commercially to produce hydrogen from water until 1902 by the Oerlikon Engineering Company. During the same period, Nernst developed the high-temperature electrolyte ZrO_2 with 15% Y_2O_3 , this being the basis for solid oxide electrolysis (SOEC) and solid oxide fuel cells (SOFC). In 1951, the first commercially available high pressure electrolyser (30 bar) was presented by Lurgi. Nowadays, low temperature electrolysis technology is available with at least 13 manufactures (3 using alkaline electrolysers and 10 using polymer membranes). On the other hand, SOEC technology is still under development. This technology attracted great interest in the 1980s because of the studies carried out by Donitz and Erdle [20], where they reported the first SOEC results within the HotElly project from Dornier System GmbH using electrolyte supported tubular SOEC. In this program, single cells have been operated during long-term periods with current densities of $-0.3 A cm^{-2}$ and 100% Faraday efficiency at a voltage as low as 1.07 V. In addition, Westinghouse Electric Corporation Research and Development Centre contributed to the development of SOEC. They reported Area Specific Resistance (ASR) values of about $0.6 \Omega cm^2$ per cell in a seven-cell stack at $1003^\circ C$ [21]. Research in high temperature

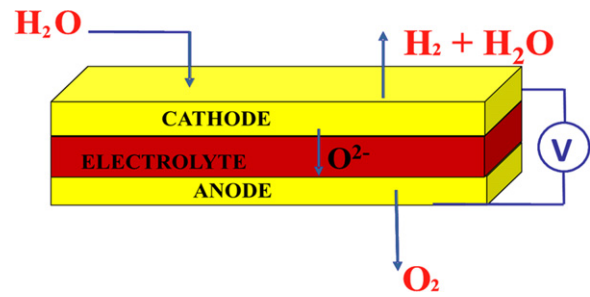


Fig. 1. Scheme of a SOFC cell operating under electrolysis mode.

electrolysis has increased significantly in recent years, as will be described in the present review.

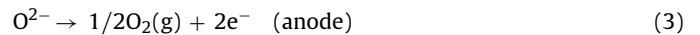
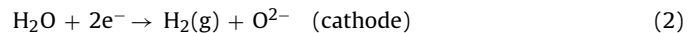
1.2. Thermodynamics

The electrochemical reactions that take part in an SOEC are the inverse reactions to those that take part in an SOFC. Cell polarization is the opposite and anode and cathode interchange their roles. In an SOEC, water acts as a reactant and is supplied to the cathode side of the cell (anode electrode in SOFC mode). Oxygen ions are transported to the anode through the electrolyte, and hydrogen is produced in the cathode side, as shown in Fig. 1.

The overall reaction of the water electrolysis is:



The reactions in the cathode and anode sides are:



There are mainly two types of electrolysers, depending on their operation temperature: low temperature electrolysers (LTE) and high temperature electrolysers (HTE). LTE are also divided into alkaline and proton-exchange membrane, and these devices are proven technologies that can achieve energy efficiencies of about 75% [22].

The major problem associated with LTEs is the high electric energy consumption which can degrade the competitiveness of the process. Although LTE is a mature technology, HTE presents a greater potential as the electrolysis of water is increasingly endothermic with increasing temperature. The required electrical power is reduced at higher temperatures as the unavoidable joule heat of an electrolysis cell is used in the H_2O splitting process. Another advantage of the high temperature is the reduction of electrode overpotentials which cause power losses in the electrolysis cell.

The minimum electric energy supply required for the electrolysis process is equal to the change in the Gibbs free energy (ΔG):

$$\Delta G = \Delta H - T \Delta S \quad (4)$$

where ΔH is the enthalpy change, T the temperature and ΔS the entropy change. The electrical energy demand, ΔG , decreases with increasing temperature; for example, the ratio of ΔG to ΔH is about 93% at $100^\circ C$ and about 70% at $1000^\circ C$.

The thermodynamics of water electrolysis are given in Fig. 2. In this figure we can observe how ΔG decreases and heat energy demand ($T \Delta S$) increases with increasing temperature at a steam pressure of 0.1 MPa. Even though total energy demand is increasing, the decrease in electrical energy demand is more noticeable, as over two thirds of the cost of electrolytic hydrogen arises from the use of electricity. Operating at higher temperature can therefore decrease the cost of the hydrogen produced, especially if the increase in heat energy demand can be fulfilled by an external heat

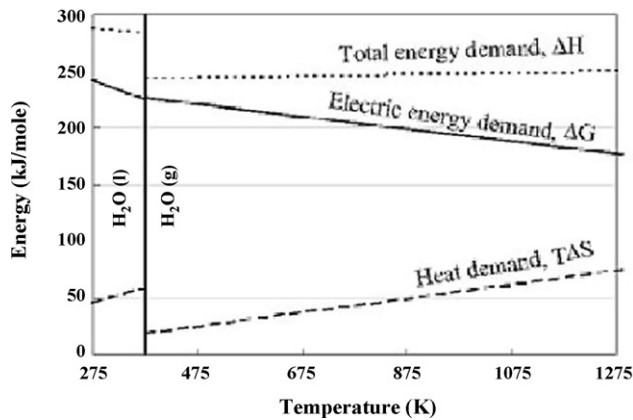


Fig. 2. Thermodynamics of water electrolysis.

According to Ref. [20]. Elsevier permission.

source, such as nuclear power, renewable energy, or waste heat from high-temperature industrial processes.

As previously described, since the thermal energy required for the electrolysis reaction can be obtained from Joule heat produced within the cell as a consequence of the passage of electrical current through the cell, the electrical energy demand is reduced and therefore the H_2 production price also decreases. For these devices, the thermoneutral potential is defined as the potential at which the generated Joule heat in the cell and the heat consumption for the electrolysis reaction are equal:

$$V_f = \frac{\Delta H_f}{nF} \quad (5)$$

where ΔH_f is the total energy demand for the electrolysis reaction, n is the number of electrons involved in the reaction and F is the Faraday constant. At the typical temperature of SOEC operation (900–950 °C), this voltage is around 1.29 V. At this level, the cell can be theoretically operated at thermal equilibrium with an electrical conversion efficiency of 100%. If we operate below the thermoneutral voltage (endothermic mode), the electric energy is lower than the enthalpy of reaction and heat must be supplied to the cell to maintain the temperature. In this mode of operation, electrical efficiencies above 100% could be achieved. On the contrary, if we operate above the thermoneutral voltage (exothermic mode), electrical efficiencies below 100% are obtained. However, operating in the exothermic mode (at moderate overpotentials) can present some advantages, for instance in wind farms during high-wind conditions and no electric demand. Although the electrical efficiency will be lower, high current densities can be obtained and therefore the hydrogen production rate will be higher.

According to Hauch et al. [23], in the case of H_2O being fed into the system as liquid water, we should also take into account the heat demand for water evaporation at 100 °C which results in an increase in the operation voltage given by,

$$V_{vap} = \frac{\Delta H_{vap}}{nF} \quad (6)$$

where ΔH_{vap} is the molar energy demand for steam raising, n is the number of electrons involved in the reaction and F is the Faraday constant. As the water vaporization enthalpy (ΔH_{vap}) is $40.65 \text{ kJ mol}^{-1}$, the voltage V_{vap} corresponds to 0.21 V. Bearing in mind that all the energy necessary to heat up the incoming gases is obtained from the outgoing gases using a perfect heat exchanger, the thermoneutral potential is then defined as the sum of both Eqs. (5) and (6), and at a temperature of 950 °C this value is about 1.5 V. In order to calculate an accurate thermoneutral point of the real

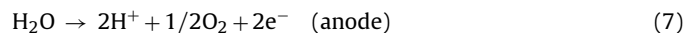
stack, more complex calculations including all heat losses will be required.

1.3. Materials for solid oxide electrolysis cells

The typical materials used in SOEC are basically similar to those used for SOFC. Detailed information of SOFC materials can be found in the following references [24–27]. The most common electrolyte material is a dense ionic conductor consisting of ZrO_2 doped with 8 mol% of Y_2O_3 (YSZ) [23]. This material presents high ionic conductivity as well as thermal and chemical stability at the operation temperatures (800–1000 °C). Other materials are also considered, such as Scandia stabilized zirconia (ScSZ) [28,29], ceria-based electrolytes (fluorite structure) [30,31] or the lanthanum gallate (LSGM, perovskite structure) materials [32,33], as will be discussed in further sections. For the fuel electrode (cathode in electrolysis mode), the most commonly used material is a porous cermet composed of YSZ and metallic nickel [23]. Other alternative materials also used for the fuel electrode include samaria doped ceria (SDC) with nickel dispersed nanoparticles [34], titanate/ceria composites [35], or the perovskite material lanthanum strontium chromium manganite (LSCM) [36]. Finally, for the oxygen electrode the most common material used to date is the lanthanum strontium manganite (LSM)/YSZ composite [23]. Different electrode materials have also been proposed, including $La_{0.8}Sr_{0.2}FeO_3$ (LSF), and $La_{0.8}Sr_{0.2}CoO_3$ (LSCO) [37]; lanthanum strontium cobalt ferrite (LSCF) and lanthanum strontium copper ferrite (LSCuF) [35]; nickelate based materials such as $Nd_2NiO_{4+\delta}$ [38] or the $Sr_2Fe_{1.5}Mo_{0.5}O_{6-\delta}$ (SFM) perovskite [39]. Although the materials typically employed for SOEC until now have been basically the same as those used for SOFC, we should take into account that operation conditions in electrolysis mode have also changed drastically. As a consequence, several issues are emerging such as example those associated with the high steam concentrations at the fuel electrode, the high oxygen partial pressures at the electrolyte/oxygen electrode interface, or the presence of electronic conduction in zirconia based electrolytes. All these issues will be discussed in more detail in further sections.

1.4. Proton conductor materials for high temperature steam electrolysis

Instead of using an oxygen conductor electrolyte, another possibility for SOEC is the use of a proton conductor. In this case, the reactions that take place in both electrodes are:



The main advantage of using proton conductors over an oxide ion conductor is that using these systems allows the production of pure and dry hydrogen gas at the cathode, whereas when using oxide conductors, the non-utilized steam is mixed with the hydrogen produced and the use of gas separators is required. This also means that proton conducting SOECs can be coupled directly with a high temperature reactor steam cycle. However, proton conductors have been proven to be able to conduct oxide ions as well as protons at higher temperatures [40]. Mixed conduction can also be beneficial for these devices, as will be discussed in the following sections.

2. Status of high temperature electrolysis using SOFC

As previously described in the introduction section, the first significant results were reported by Donitz et al. in the 1980s [20,22,41,42]. The HotElly project (High Operating Temperature Electrolysis) system was led by Dornier GmbH, and consisted of

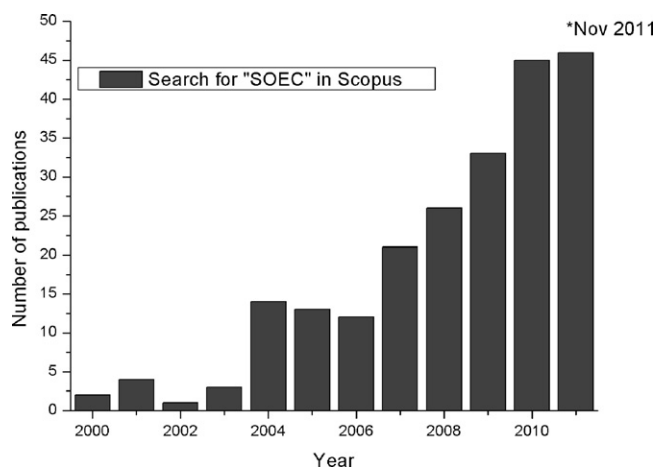


Fig. 3. Number of publications per year in SOEC according to Scopus database.

research into electrolysis single cells as well as pilot plant tests. They used the typical materials: YSZ (8–12 mol% Y_2O_3) electrolyte (thickness of 300 μm), LSM (250 μm) as the oxygen electrode, Ni-YSZ cermet (100 μm) for the fuel electrode, and doped lanthanum chromite as interconnectors. Their system consisted of electrolyte supported ring cells connected in series. For example, they obtained a hydrogen production rate of about 600 N l h^{-1} using mixtures of 20% steam/80% hydrogen in a 100-tube module with a current value of 14 A and voltage of 13.2 V at 1000 °C [43]. The mean cell voltage for the system is 1.3 V, being thermodynamically self-sustaining at this voltage. They also claimed that their system can be operated in either endothermic or exothermic mode. In the endothermic mode, the system requires less electricity and thus obtains higher efficiency, but the inlet gas must be preheated to the operation temperature. Operating in exothermic mode, more electricity is required, but in this case the electrolyser produces excess heat which could be used to heat the inlet gases. As part of the same project, Erdle et al. [42] demonstrated the feasibility of 32 electrically series-connected tubular cells for both SOFC and SOEC modes at a standard operating temperature of 1000 °C.

Westinghouse Electric also developed a tubular electrolyser using the same design as they had for SOFC. They used a porous calcia stabilized zirconia (CaSZ) supporting tube (1–1.5 mm in thickness), LSM as the oxygen electrode (1.4 mm), 10YSZ as the electrolyte (40 μm) and Ni-YSZ as the fuel electrode. They obtained a hydrogen production rate (single cell operating at 1000 °C) of 17.6 N l h^{-1} at 1.23 V and 0.4 A [44].

Probably due to the low oil prices relatively few research works were performed in the 1990s, where the only remarkable works were done in Japan [30,45]. However, research on SOEC has grown exponentially in the last decade, as observed in the plot of Fig. 3. Companies and research centers such as Ceramtec Inc. and several universities in the US, CEA in France, EIfER in Germany, Topsø Fuel Cell and Risø in Denmark, Imperial College London, INET in China and Kyushu University in Japan, are just a few examples of the recent activity in the field. Another remarkable project funded by the European Commission is the Relhy project [46], including 7 European partners. This project is focussed on the development of novel or improved, low cost materials, the associated manufacturing process, and for their integration in efficient and durable components for the next generation of electrolysers based on SOEC.

2.1. Zirconia based SOEC

2.1.1. Yttria doped zirconia electrolytes

As well as for SOFC, doped zirconia is the most commonly used material for SOEC applications. Apart from the HotElly project and

that of Westinghouse Electric in the 1980s previously mentioned, Momma et al. [45] also investigated the behavior of SOEC cells and compared it with that of SOFCs using YSZ-based planar discs. They observed that Ni-YSZ cermet fuel electrode presents asymmetric behavior indicating the existence of diffusion limited process in the electrolysis direction. For the oxygen electrode, they also observed degradation behavior which ended up with electrode delamination from electrolyte, and the degradation rate decreased using a mixed ceria intermediate layer between YSZ and the electrode.

Researchers at the Energy Research Centre of the Netherlands (ECN) have also studied YSZ-based solid oxide electrolysers [47]. They used the state of the art SOFC materials for both air-assisted and hydrocarbon-assisted hydrogen production and found similar ASR-cell values in electrolysis and fuel cell modes for electrolyte supported cells (90 μm thick 3YSZ electrolyte, Ni-GDC fuel electrode and LSM-YSZ or LSCF as the oxygen electrode) measured at temperatures between 650 °C and 920 °C. They have also tested fuel electrode supported cells (5 μm thick 8YSZ electrolyte) and obtained lower ASR-cell values, although hydrogen production was limited at steam utilizations of 50% due to transport limitations of the substrate.

Remarkable work on YSZ based SOECs has also been done at the European Institute for Energy Research (EIfER) in Karlsruhe (Germany). They have performed electrolysis studies up to 160 h in a commercial SOFC from HTCeramic (Switzerland) and no apparent degradation was detected [48]. Their experimental set-up for the measured cells can be observed in Fig. 4 (left). For example, at 900 °C and 82 vol% of absolute humidity (AH) they have measured a current density of -1.4 A cm^{-2} at 1.1 V (ASR values are about $0.20 \Omega \text{ cm}^2$), which corresponds to electrical cell efficiency above 100%, being this a great improvement in comparison with alkaline electrolysis. They have also observed similar cell impedance values for both SOFC and SOEC, probing the reversibility of the cells. Their experimental results concluded that SOEC operation was limited by gas diffusion at the fuel electrode, especially at humidities below 70 vol% AH (Fig. 4 right) and thus, optimization of the fuel electrode will be required for an industrial scale implementation.

Uchida et al. [34] performed electrolysis tests in different types of cells. They used Ni-YSZ or platinum for the fuel electrode, YSZ or SDC for the electrolyte, and LSM or LSC for the oxygen electrode. They concluded that Ni-YSZ is preferable due to better adhesion with the YSZ electrolyte, although it shows degradation caused by the high steam concentrations under operating conditions and as a consequence, Ni particles seem to be oxidized. For the oxygen electrode, LSM presents much lower activity for oxygen evolution due to low concentration of oxygen vacancies, and in some cases delamination was observed. They have also observed that YSZ is stable in electrolysis mode. However, for SDC electrolytes, the high applied voltage inevitably leads to the reduction of Ce^{4+} to Ce^{3+} , deteriorating the ionic transference number. Thus, the unsteady electrolysis of ceria proceeded from the hydrogen electrode side and therefore ceria cannot be used as the electrolyte for SOEC applications.

SOFCs fabricated at Risø National Laboratory have also been tested in electrolysis mode obtaining excellent results [49]. Their planar cells consist of Ni/YSZ support (300 μm), Ni/YSZ active layer, YSZ electrolyte (10–15 μm), and a 15–20 μm thick strontium-doped lanthanum manganite/YSZ composite oxygen electrode. They have performed a complete analysis of studies as a function of the temperature and gas compositions, and detailed information can be found in Refs. [23,49,74,75,98]. They concluded that their cells can be operated as both fuel cell and electrolysis mode, and as an example, they have measured an ASR_{cell} as low as $0.15 \Omega \text{ cm}^2$ at 950 °C using 50% $\text{H}_2\text{O}/50\% \text{H}_2$ as fuel at the hydrogen electrode.

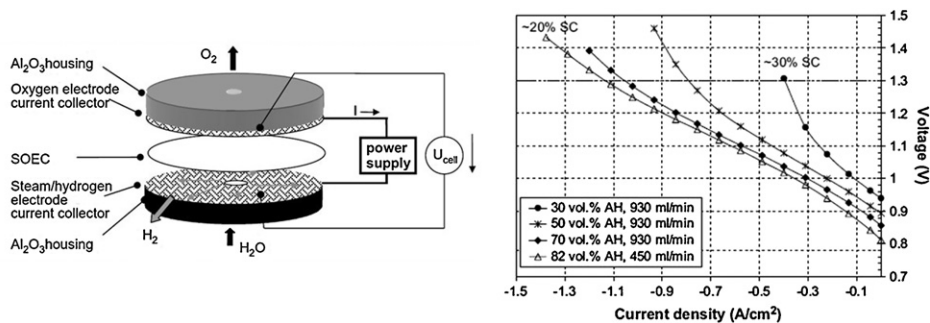


Fig. 4. (Left) experimental set-up for SOEC measurements according to Ref. [48] and (right) j - V curves in electrolysis mode at 800 °C as a function of the composition of the gas supplied to the fuel electrode site.

According to Ref. [48]. Elsevier permission.

2.1.2. Scandia doped zirconia electrolytes

Although YSZ is the most common electrolyte material for SOFC applications due to its high ionic conductivity and chemical stability, other materials have been proposed in recent years such as the Scandia-stabilized zirconia (ScSZ), which presents higher ionic conductivity compared to the standard YSZ, and thus it is possible to decrease the cell operation temperature.

Currently there is also strong interest in hydrogen production by HTSE at Ceramtec, Inc. in collaboration with Idaho National Laboratory (INL) [28]. They have published single cell-electrolysis measurements in 2005, in collaboration with O'Brien et al. from INL. They have performed electrochemical tests using both YSZ and scandia (4 mol%)-stabilized zirconia (4ScSZ) electrolyte supported cells over a temperature range of 800–900 °C. Details of their experimental setup and single cells can be observed in Fig. 5. As an example, for the 4ScSZ (125 μm thick) they have measured ASR values of about 0.33 and 0.50 $\Omega\text{ cm}^2$ at 850 °C and 800 °C, respectively. They also observed that cell performance was continuous from the fuel-cell mode to the electrolysis mode of operation. However, they also observed ASR degradation that was associated with thermal cycling of the cell.

ScSZ cells were also tested at Imperial College London [29], where they have measured electrolyte supported Scandia (10 mol%) and ceria (1 mol%) stabilized zirconia (10Sc1CeSZ) using Ni/YSZ as the fuel electrode and platinum as the oxygen electrode. At 900 °C and using 80% RH (relative humidity) of steam at the fuel electrode site they have measured current densities of -450 mA cm^{-2} at 1.5 V (ASR = 0.99 $\Omega\text{ cm}^2$).

2.2. Ceria based electrolytes

Ceria electrolytes are probably the most promising electrolyte for intermediate temperature SOFC. Cerium oxide is usually doped with Gd_2O_3 (GDC) or Sm_2O_3 (SDC) to produce the ionic conductivity, which is higher than which corresponds to the YSZ. However, relatively few investigations have been done using ceria based material under electrolysis mode, possibly due to the partial reduction of Ce^{4+} to Ce^{3+} under operation.

Eguchi et al. [30] have investigated a planar SDC based cell under electrolysis mode and compared it with YSZ based electrolytes. Although the use of ceria led to lowering both hydrogen electrode and oxygen electrode overvoltages compared to YSZ based cells, the high applied voltages leads to the reduction of Ce^{4+} to Ce^{3+} and deteriorating the ionic transference number. They concluded that ceria electrolyte cannot be used as an electrolyte for electrolysis applications.

Electrolysis experiments on ceria-based composite electrolyte cells were also performed by Zhu et al. [31]. They have

used an SDC-carbonate composite (63 mol% 20SDC-24 mol% Li_2CO_3 -13 mol% Na_2CO_3) electrolyte based cell using Pt as both fuel and oxygen electrodes. Those ceria based composites (CBCs) have been developed to overcome the shortcomings that typically occur in the ceria single-phase electrolytes. They have demonstrated that the CBCs present both proton and oxygen ion conduction and are also effective for both fuel cell and electrolysis applications. The fuel cell performance at 650 °C was around 0.38 W cm^{-2} . The electrolysis measurements for both H^+ and O^{2-} conduction modes showed typical electrolysis behavior, and the observed decomposition voltages were 1.0 and 1.75 V for the H^+ mode and the O^{2-} mode, respectively.

The use of composite electrolytes was also recently proposed by Kim-Lohsoontorn et al. [50]. They used a bi-layered GDC/YSZ electrolyte and compared it to a GDC and YSZ electrolyte. Ni-GDC was used as an H_2 electrode while LSM-YSZ was used as an O_2 electrode. As observed in Fig. 6, the bi-layered YSZ/GDC electrolyte cell exhibited significantly higher performance when compared to the cell using YSZ or GDC electrolyte. They have also investigated the performance of the cell under CO_2 electrolysis, and comparable performance was observed. Further experiments will be required to assure the stability of these materials.

2.3. LaGaO₃ based electrolytes

LaGaO₃ based oxide electrolytes, usually doped with Sr on the La site and Mg on the Ga site (LSGM) are also considered to be as one of the most promising oxide ion conductor for intermediate temperature SOFCs. LSGM has also been proposed for SOEC applications using $\text{La}_{0.8}\text{Sr}_{0.2}\text{CoO}_{3-\delta}$ (LSCo) for the oxygen electrode and $\text{Ni}_{1-x}\text{Mg}_x\text{O}$ -ceria composite for the fuel electrode [51]. At 800 °C and using 56% RH they have measured an ASR of around 0.6 $\Omega\text{ cm}^2$. They have also fabricated an electrolyte-supported 10-cell stack using nickel-based superalloy as the interconnect material. The measured ASR in both fuel cell and electrolysis mode was about 1 $\Omega\text{ cm}^2$.

Ishihara and Kanno [52] also studied LSGM based electrolyte materials for steam electrolysis applications. They examined different electrodes and found that bimetallic Ni-Fe (9:1) and $\text{Ba}_{0.6}\text{La}_{0.4}\text{CoO}_3$ (BLC) showed the smallest overpotentials for both fuel electrode and oxygen electrode, respectively. In particular, the addition of Fe to the Ni fuel electrode was found to be very effective for improving the electrolysis performance of the cells by decreasing the IR loss and the cathodic overpotential. They also concluded that both hydrogen and oxygen production rates almost follow the estimated Faraday's law value and the current density up to 1.8 V. Of great interest are their estimations about the energy balance of the cell based on the measured performance. They concluded

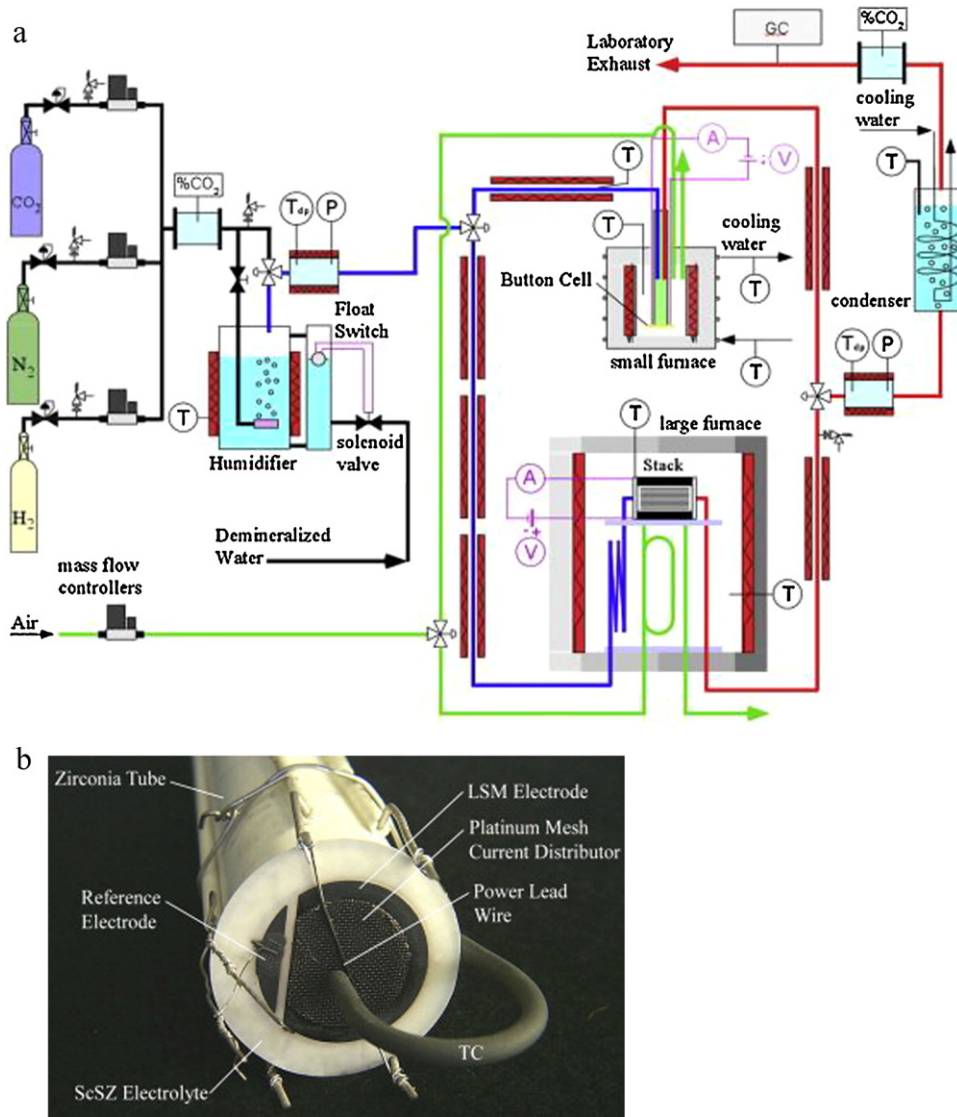


Fig. 5. Experimental set-up [140] and detail of a single cell [135] measured at INL.

Elsevier permission.

that the unused Joule heat when operating under exothermic mode could be used for the heat source of the steam generation, and from these results, even the steam at 150 °C level could be used for this purpose.

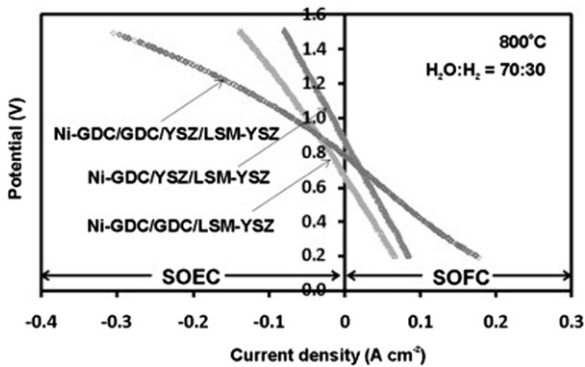


Fig. 6. *j*-*V* curves of the cells having different electrolytes (YSZ, GDC, and bi-layered GDC/YSZ electrolyte) in the steam electrolysis and SOFC modes measured at 800 °C. According to Ref. [50]. Elsevier permission.

2.4. Proton conducting electrolyte materials

Proton conductors for SOFC applications are under continuous development [53–56], although they still have problems associated with chemical stability and also with the integration with other cell components. In electrolysis mode, as stated before, the main advantage of these systems is that pure hydrogen is produced, and the fuel is not diluted with water vapor as in the case of using an oxide ion conductor. Detailed information regarding protonic conduction for SOEC applications can be found in Ref. [57]. Proton conductors were first proposed for steam electrolysis applications over 30 years ago by Iwahara et al. [58]. They studied the performance of the $\text{SrCe}_{1-x}\text{M}_x\text{O}_{3-\delta}$ system ($x=0.05-0.10$, $M = \text{Yb, Mg, Sc, Y, In, Zn, Nd, Sm, Dy}$) using Pt electrodes. Measuring the hydrogen evolution by gas chromatography they confirmed the protonic conduction of the cell in electrolysis mode. They obtained current efficiencies for hydrogen production of about 50–95% in the range of 0.1–0.8 A cm^{-2} at 900 °C. The overvoltage, with the exception of ohmic losses, was less than 0.3 V at a current density of -0.4 A cm^{-2} . Any current that causes electron–electron hole recombination, arising from electronic conduction in the electrolyte, will reduce the current efficiency for H_2 production. High applied voltages were

necessary to produce hydrogen and they concluded that losses were largely due to ohmic losses.

Matsumoto et al. [59] also found that ohmic loss was the main contributor to the overall losses during their experiments. Steam was electrolyzed at 800 °C using a cell made from $\text{SrCe}_{0.95}\text{Yb}_{0.05}\text{O}_{3-\delta}$ electrolyte and Pt electrodes. Hydrogen evolution was less than the theoretical maximum with the proton transport number measured to be as low as 0.6. It was suggested that the low proton transport number may have been caused by a low $p\text{H}_2\text{O}$ in their experiments.

Kobayashi also tested a steam electrolysis cell using the proton conductor $\text{SrZr}_{0.9}\text{Yb}_{0.1}\text{O}_{3-\delta}$ as an electrolyte [60]. This electrolysis cell was able to reduce nitrogen oxide (NO) using the produced hydrogen by steam electrolysis as a reducing agent at around 460 °C. When using $\text{Pt}/\text{Ba}/\text{Al}_2\text{O}_3$, where barium is known to absorb NO effectively to produce nitrate, the reduction of NO was accelerated, and the reduction even takes place under oxygen excess. They also found that, when using an oxide ion conductor such as the YSZ, the reduction of the NO is not possible in the cell due to the coexistence of NO and O_2 . In this case, oxygen reduction takes place before the reduction of NO and the steam electrolysis, which could provide hydrogen as an effective reducing agent for NO.

Irvine et al. also patented a steam electrolyser using a proton conducting electrolyte [61]. Many proton conducting materials were suggested for their use as the electrolyte material including yttrium doped-barium cerate (BCY), yttrium doped-barium zirconate (BZY) and the cerate–zirconate $\text{BaCe}_{0.9(1-x)}\text{Zr}_x\text{Y}_{0.1}\text{O}_{3-\delta}$ (BZCY). The device was designed to operate between 500 and 700 °C with an electrolyte thickness of no more than 25 μm . They also suggested porous platinum as the cathode, however there is no suggestion of any specific material for the anode.

Recently, Stuart et al. [62] also reported on $\text{BaCe}_{0.9}\text{Y}_{0.1}\text{O}_{3-\delta}$ (BCY10) and $\text{BaZr}_{0.9}\text{Y}_{0.1}\text{O}_{3-\delta}$ (BZY10) as electrolytes for proton conducting SOECs. Although their performance is relatively poor in comparison with the oxide ion conducting SOECs, BCY10 has been confirmed as a suitable electrolyte material for a reversible proton conducting SOFC, even though large losses were observed at lower temperatures in electrolysis mode, this being attributed to the slow progression of reactions at the electrodes.

Sakai et al. also reported on steam electrolysis using protonic conductors [63]. They used $\text{SrZr}_{0.9}\text{Y}_{0.1}\text{O}_{3-\delta}$ (SZY-91) or $\text{SrZr}_{0.5}\text{Ce}_{0.4}\text{Y}_{0.1}\text{O}_{3-\delta}$ (SZCY-541) as an electrolyte and different electrode materials, such as porous platinum or $\text{Sr}_{0.5}\text{Sm}_{0.5}\text{CoO}_3$ (SSC-55) for the anode and nickel for the cathode. In some cases they also used a $\text{SrCe}_{0.95}\text{Yb}_{0.05}\text{O}_{3-\alpha}$ (SCYb) interlayer. They found that the SSC-55 anode showed good performance, and the SCYb interlayer was effective for enhancing the activity of the nickel cathode, providing low electrode overpotentials and improving the current efficiency of the steam electrolysis due to the suppression of the partial electronic current, as usually occurs in cells with platinum electrodes. When using SZCY-541 as the electrolyte, the partial substitution of cerium for zirconium in the electrolyte was also found to be effective in terms of improving current efficiency. As a consequence, the combination of an SSC-55 anode, a nickel cathode, an SCYb interlayer and the SZCY-541 electrolyte was found to provide a current efficiency of about 100% up to 100 mA cm^{-2} at both 600 and 800 °C, and the hydrogen evolution rate was about 25 $\mu\text{m min}^{-1} \text{cm}^{-2}$.

Finally, He et al. [64] also reported on the performance of the protonic conductor $\text{BaCe}_{0.5}\text{Zr}_{0.3}\text{Y}_{0.2}\text{O}_{3-\delta}$ electrolyte in electrolysis mode. As an example, at 700 °C they achieved electrolysis current densities of about -830 mA cm^{-2} at 1.5 V using 50% H_2O –air and H_2 as reacting gases at the oxygen electrode and hydrogen electrode, respectively. They also studied the electrochemical response of the electrolysis cells by AC impedance. Their results suggest that the surface diffusion of oxygen adsorption is not the elementary

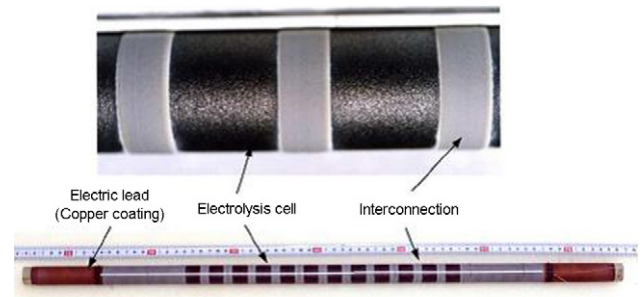


Fig. 7. Outer view of a tubular SOEC cell. According to Ref. [66]. Elsevier permission.

step for SOEC reaction, which was in concordance with the low frequency resistance observed in their cells.

It was also suggested that the transfer of protons involves two steps in SOEC mode: the protons decomposed from water transferring to the triple phase boundaries (TPBs) and the protons at the TPBs transferring to the electrolyte, which might be the reason for the large high frequency resistance observed in their case.

2.5. Alternative designs for solid oxide electrolysis cells

Most of the designs previously mentioned are based on planar technology, which is the most used in both SOFC and SOEC. However, innovative designs have also been proposed for SOEC applications. Doenitz and Erdle firstly proposed the tubular configuration for SOEC applications [20].

Another innovative tubular design was reported by Hino et al. [65,66]. Their tube was composed of 12 electrolysis cells, each of 19 mm in length and connected in series, as observed in Fig. 7. Ni/YSZ cermet was used as the fuel electrode and LaCoO_3 as the oxygen electrode. Using this design they achieved a maximum hydrogen production rate of 6.9 N l h^{-1} at 15.6 V, 1.72 A and 950 °C, and the total ASR was about 9 Ω . The energy efficiency was about 77%, which can be mainly attributed to the low oxygen conductivity at this temperature, as the thickness of the YSZ was about 300 μm . Another possible explanation for the low Faraday efficiency could be the high ohmic losses at the interconnectors and electric lead layers and/or an increase of the concentration overvoltage due to gas transport limitations of steam along the supporting tube. In addition, large parts of the oxygen electrode layers were separated from the electrolyte. In fact, delamination of the oxygen electrode is one of the main limitations in SOEC, as will be discussed in further sections.

Metal supported cells fabricated at DLR (Deutsches Zentrum für Luft- und Raumfahrt) in Germany have also been recently proposed for SOEC applications [67]. Their cells, fabricated by plasma deposition, consist of a porous ferritic steel support, a diffusion barrier layer of $\text{La}_{0.7}\text{Sr}_{0.15}\text{Ca}_{0.15}\text{CrO}_3$, a Ni/YSZ hydrogen electrode, a YSZ electrolyte and an LSCF oxygen electrode. For example, at 800 °C using 70% hydrogen/30% steam as the fuel electrode, the cell voltage at a current density of -1 A cm^{-2} was about 1.4 V and at 850 °C as low as 1.28 V. They have also performed a long-term test of up to 2300 h using a constant current density of -0.3 A cm^{-2} at 800 °C, starting after 394 h and using 43% RH for the whole test. During the first 1000 h, the cell voltage increased by 2.1% 1000 h^{-1} , and during the next 1000 h, the degradation increased to 3.9% 1000 h^{-1} , which is slightly higher than the standards for SOFC (1% 1000 h^{-1}). They have also performed microstructural studies after operation and found certain oxidation of the ferritic steel substrate, and small migration of Fe and Cr into the hydrogen electrode.

Microtubular configuration has also attracted great interest in recent years for SOFC applications [68–70]. This configuration

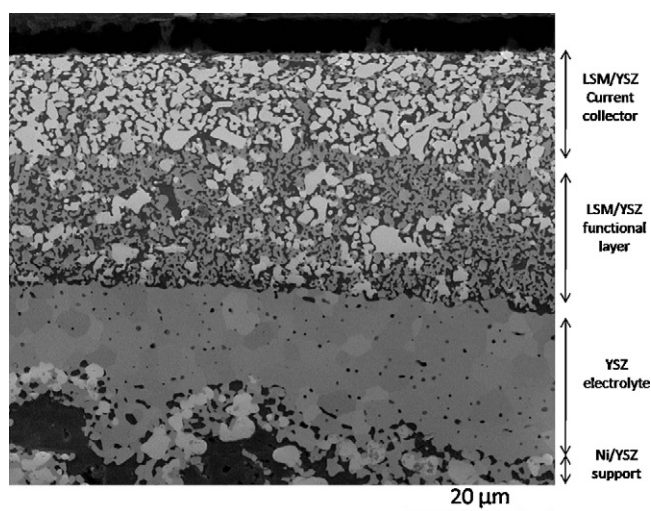


Fig. 8. Microstructure of a microtubular SOEC prior to electrolysis operation according to Ref. [73].

presents several advantages compared to the traditional design, including increased power density per unit volume, easy sealings, and shorter start-up and shut-down time, due to their resistance to thermal cycles, and as a consequence, less redox-cycling damage. Steam electrolysis using microtubular configuration was reported by Hashimoto et al. [71]. They used a Ni–ScSZ supporting tube, ScSZ electrolyte, GDC as a buffer layer and LSCF–GDC as the oxygen electrode. Using 18% RH of steam at the fuel electrode site, they observed a cell voltage of 1.37 V at 0.1 A cm^{-2} and 700°C , which corresponds to an ASR of $4.3 \Omega \text{ cm}^2$. Although their performance is relatively low in comparison with the standards in planar SOEC, they have demonstrated the feasibility of the microtubular configuration for SOEC applications.

A different microtubular SOEC system was also recently studied [72,73]. They reported reversible microtubular cells consist of Ni/YSZ support YSZ electrolyte and LSM/YSZ as the oxygen electrode (Fig. 8). At current densities of -1 A cm^{-2} and using 70% RH of steam as the fuel, they obtained a voltage of 1.3 V at 850°C . At higher voltages, the cell resistance drops and high current densities can be supported by the cell. The reason for this effect is YSZ electroreduction and as a consequence, YSZ becomes a mixed ionic and electronic conductor. In addition, this process was found to be reversible. Those findings will be also further discussed in following sections.

2.6. Electrode materials for SOEC applications

2.6.1. Fuel electrodes for SOEC

Although Ni/YSZ is the most common material for both SOFC and SOEC applications, several authors have reported on the degradation of this material under electrolysis applications [74–76]. As well as this, small amounts of hydrogen are required on the fuel electrode side in order to avoid the reoxidation of Ni to NiO. The need for hydrogen in order to produce hydrogen could result in incongruousness. As well as in SOFCs, novel materials are continuously being proposed as candidates for the fuel electrode in SOECs. Marina et al. [35] reported on the performance of the lanthanum-substituted strontium titanate/ceria composite as the fuel electrode. They found that titanate/ceria composite electrodes seem to be more active than the standard Ni/YSZ composite for steam electrolysis applications. In particular, they found that under high steam and low hydrogen partial pressures, the Ni/YSZ suffers irreversible degradation.

Researchers from the Watanabe group in Japan also presented an alternative using a highly dispersed nickel–SDC catalyst [34,77]. They found that the Ni-dispersed SDC fuel electrode presented the highest performance at 17 vol% of nickel loading due to the effective enhancement of the reaction rate by increasing the active reaction sites and lowering the electronic resistance. In addition, the increase of the electrode activity was found to increase the ionic conductivity of the zirconia electrolyte. The authors measured a cell consisting of Ni-dispersed SDC fuel electrode, ScSZ electrolyte, SDC interlayer and LSCO as the oxygen electrode and obtained 1.13 V at -0.5 A cm^{-2} and 900°C under 60% RH of steam.

Yang and Irvine [36] recently proposed the novel perovskite material $(\text{La}_{0.75}\text{Sr}_{0.25})_{0.95}\text{Mn}_{0.5}\text{Cr}_{0.5}\text{O}_3$ (LSCM) as the fuel electrode for steam electrolysis cells. They used a porous YSZ electrode support impregnated with LSCM as the fuel electrode, YSZ as the electrolyte and YSZ porous and impregnated LSF as the oxygen electrode. They concluded that LSCM could be an alternative to standard Ni/YSZ electrodes for SOEC applications, although further work is necessary to improve electrode microstructure and current collection as well as to explore the partitioning of processes related to the conditioning of electrodes. In addition, chemical changes were observed, possibly due to reduction of the LSCM perovskite phase.

2.6.2. Oxygen electrodes for SOEC

It is known that long term degradation in SOFC occurs faster than in SOEC, and this fact is possibly related to the oxygen electrode. During steam electrolysis, high oxygen partial pressures occur at the electrode/electrolyte interface and thus, delamination of oxygen electrodes is one of the major degradation issues in SOEC [78,79]. A typical example of the oxygen electrode delamination can be observed in Fig. 9. Development of novel oxygen electrodes are required in order to improve their phase stability and the electrode/electrolyte interface under high oxygen partial pressures during SOEC operation.

Several efforts have been made in order to optimize the performance of the oxygen electrodes. As previously stated, LSM–YSZ is (as in SOFC) the most common material used as the oxygen electrode [23]. Liang et al. [80] studied the activation mechanism of the LSM–YSZ composite when operating in a SOEC. They found that an anodic current treatment of the cell could significantly enhance the electrochemical activity of the electrodes, as seen by other authors in SOFC, where the application of cathodic polarization also enhances the activity of the LSM electrode [81]. Based on previous investigations, they developed a model for the activation/deactivation of the LSM–YSZ under SOEC mode. Under anodic polarization, manganese ions at the LSM lattice are reduced and SrO is incorporated into the LSM lattice and thus, it was suggested that generation of oxygen vacancies are produced at the LSM–YSZ electrode enhancing the transport and diffusion of oxygen ions. Another possible mechanism for this effect was proposed by Backhaus-Ricoult et al. [82]. They observed that there is a strong enrichment of the YSZ surface in Mn^{2+} that provides high electronic conductivity in the zirconia surface region promoting the direct incorporation of oxygen from the oxygen gas into the electrolyte. These explanations are probably the reason for the good performance of the LSM/YSZ in SOEC mode, as reported by several authors [49,72,83]. On the other hand, Wang et al. [37] reported that LSM–YSZ composites showed good performance only after cathodic activation because this activated state is lost during operation under SOEC mode, LSM-based electrodes do not appear to be optimal, which is also in concordance with the results of Chen et al. [84]. Recently, Chen et al. [85] also developed GDC-impregnated LSM oxygen electrodes for SOEC. The addition of GDC nanoparticles enhances the electrochemical activity for the oxygen evolution, which is consistent with several reported results in SOFCs [86,87]. Furthermore, the addition of the GDC nanoparticles

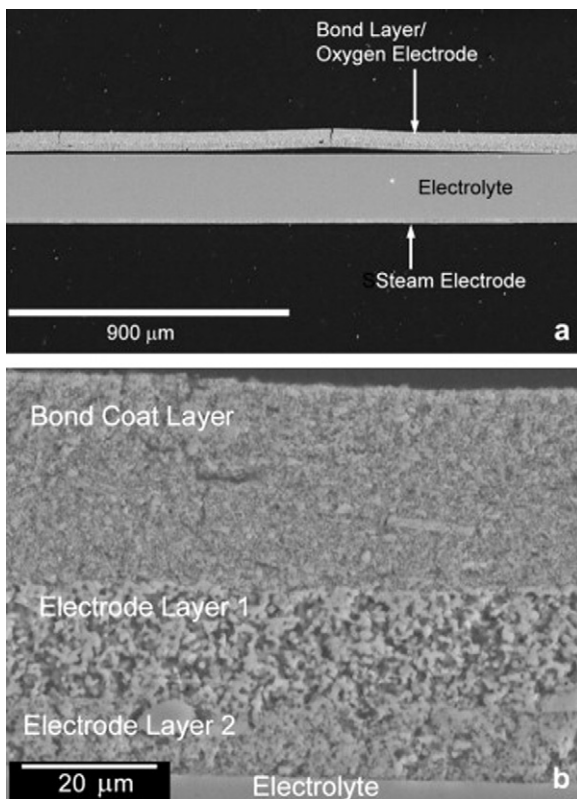


Fig. 9. SEM micrographs of a polished cross-section of a cell from the 2000-h stack (near the oxygen exit, steam inlet corner): (a) area where the oxygen electrode delaminated, (b) area where the bond-coat and oxygen electrode are still attached to the electrolyte.

According to Ref. [97]. Elsevier permission.

also inhibits the delamination of the oxygen electrode from the YSZ electrolyte, as observed for pure LSM. However, further experiments are required to fully understand the mechanisms of the LSM/YSZ and LSM/GDC composites under SOEC conditions.

Alternative oxygen electrodes are continuously being proposed. For example, Wang et al. [37] also tested different composite electrodes of YSZ with $\text{La}_{0.8}\text{Sr}_{0.2}\text{FeO}_3$ (LSF), and $\text{La}_{0.8}\text{Sr}_{0.2}\text{CoO}_3$ (LSCo) as SOEC oxygen electrode. They found that LSF–YSZ and LSCo–YSZ composites exhibit impedances that are essentially independent of current and are almost identical under anodic and cathodic polarization. Kong et al. [88] also found that LSF–YSZ composites exhibit high catalytic activity to oxygen evolution, in comparison with LSM–YSZ.

In addition, Marina et al. [35] studied a wide range of oxygen electrodes, including mixed ion- and electron-conducting (MIEC) lanthanum strontium ferrite (LSF), lanthanum strontium copper ferrite (LSCuF), lanthanum strontium cobalt ferrite (LSCF), as well as LSM. In general, they demonstrated that oxygen electrodes performed less well for oxygen evolution than oxygen reduction. This behavior was most apparent for the MIECs LSCuF and LSCF electrodes, while the effect was less, although still discernable, for LSM. These observations are consistent with an expected decrease in the oxygen vacancy concentration when changing from SOFC to SOEC mode. LSCF as the oxygen electrode for SOEC applications has also been tested and proposed by other authors [67,71,89,90].

Another alternative is the perovskite $\text{Sr}_2\text{Fe}_{1.5}\text{Mo}_{0.5}\text{O}_{6-\delta}$ (SFM), as proposed by Liu et al. [39]. The SFM material was prepared by a microwave-assisted combustion method in air and employed as both fuel and oxygen electrode in a symmetrical cell. For the electrolyte, they employed the LSGM perovskite. The measured ASR of the cell at OCV using 60% RH was as low as $0.26 \Omega \text{ cm}^{-2}$ at 900°C .

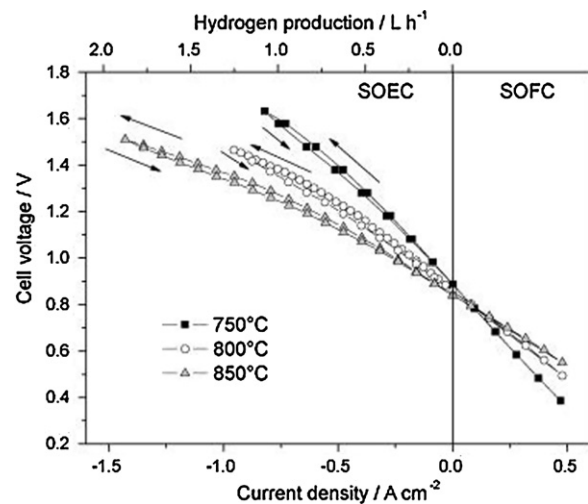


Fig. 10. j - V curves at different temperatures for a $\text{Nd}_2\text{NiO}_{4+1}$ based cell. According to Ref. [38]. Elsevier permission.

A current density of -0.88 A cm^{-2} was also achieved at 900°C and 1.3 V. The authors claim that SFM could be a very promising oxygen electrode material for SOEC applications; however, stability and durability studies will be required prior to the practical application of the material.

$\text{Ba}_{0.5}\text{Sr}_{0.5}\text{Co}_{0.8}\text{Fe}_{0.2}\text{O}_{3-\delta}$ (BSCF) was previously studied as an oxygen electrode for SOFCs and is now also proposed for electrolysis applications [91]. They claimed an ASR for the BSCF/YSZ composite as low as $0.077 \Omega \text{ cm}^{-2}$ at 850°C , and also exhibited much better performance in both SOFC and SOEC modes in comparison with the standard LSM material. BSCF was also studied in SOEC by Kim-Lohsoontorn et al. [92]. However, they found a decrease in performance when operating under SOEC mode, compared to a relatively stable LSM–YSZ cell. They observed a microstructural change in the BSCF electrode, this being the origin of the degradation. In conclusion, more stability and durability studies are required prior to the practical application of the material as an oxygen electrode for electrolysis cells.

Tao et al. [93] recently developed a double layer-type (catalyst layer/current collecting layer) oxygen electrode for reversible SOFC applications. As the catalyst layer interfaced with an SDC interlayer/YSZ solid electrolyte, mixed conducting LSCF and SDC particles were employed. They used a current collecting porous LSCF layer that was formed on the catalyst layer. They proposed that by controlling the SDC content, as well as the thickness and porosity of the catalyst layer, the gas diffusion rate and the conduction networks for electrons and oxide ions were optimized, resulting in a marked reduction of the overpotential. They found an overpotential of 0.08 V at -0.5 A cm^{-2} and 900°C under pure O_2 , which is a higher performance compared to single-layer electrodes.

Also of great interest are the K_2NiF_4 structure type materials, such as the $\text{Ln}_2\text{NiO}_{4+\delta}$ ($\text{Ln} = \text{La}, \text{Nd}, \text{Pr}$). The capability of these materials to accommodate oxygen excess is believed to favor the catalytic activity of oxygen electrodes in SOEC mode for oxygen evolution. Chauveau et al. [38,94] firstly proposed the neodymium nickelate ($\text{Nd}_2\text{NiO}_{4+\delta}$) as an oxygen electrode for electrolysis applications. They tested this material in a single cell using 3YSZ as the electrolyte and Ni–GDC as the hydrogen electrode in both SOFC and SOEC modes and found slightly lower ASR values in electrolysis mode, as observed in Fig. 10. They measured current densities of about -0.87 A cm^{-2} at 850°C and 1.3 V using 31% RH of steam at the fuel electrode site. Another material from the same family, $\text{La}_{1.7}\text{Sr}_{0.3}\text{Co}_{0.5}\text{Ni}_{0.5}\text{O}_{4.08}$ (LSCN), has also been recently proposed as an SOEC electrode [95]. Although electrolysis studies were

performed using as little as 3% RH of steam at the fuel electrode, the authors also found lower ASR values when operating in SOEC mode compared to SOFC mode. They also suggest that the hyperstoichiometry of the LSCN phase is probably the cause of the good oxygen evolution in SOEC mode.

3. Materials degradation issues in solid oxide electrolysis cells

As previously mentioned, long term degradation is the main issue for the viability of this technology as a practical hydrogen production system. Several long-term degradation studies have been performed to date and all of them have concluded that further improvements are required prior to commercialization.

For example, aging studies of metal supported cells at DLR [67] showed a degradation rate of 3.2% per 1000 h at 800 °C, -0.3 A cm^{-2} and using 43% RH of steam at the fuel electrode. Their AC impedance studies showed enhanced polarization resistance during electrolysis compared to fuel cell operation, and this was attributed to the hydrogen electrode.

Aging studies up to 1300 h were also made at Risø at 850 °C, -0.5 A cm^{-2} and 50% RH of steam, showing a degradation rate of 2% [74]. They observed by AC impedance that the degradation was also mainly attributed to the Ni/YSZ electrode. By SEM they also found the growth of Ni particles as well as the presence of Si impurities possibly, related to the variation in the electrolysis operation conditions [75].

Post-mortem analyses after 1080 h of SOEC operation in a 720-cell stack from INL were also reported [96]. In this case, the hydrogen electrode (Ni-YSZ) was mainly in good condition apart from relatively few silicon impurities coming from the seal. A transition to the monoclinic phase was detected near the edges in some cases for the 6ScSZ. They also observed the presence of Cr-doped Al_2O_3 near the seals coming from the bipolar plates and cation diffusion at the oxygen electrode. In addition, their biggest

degradation issue is the delamination of the oxygen electrode due to the high oxygen partial pressures at the electrode/electrolyte interface, as observed by other authors [45,97].

Short-term degradation is also frequent in SOEC cells, especially operating under extreme conditions such as high current densities or high steam concentration at the fuel electrode. Matsui et al. [76] studied the influence of the fuel humidity on the performance and stability of the Ni-YSZ fuel electrode at 1000 °C, and for high steam concentrations they found the formation of steam or hydroxide layers at the cermet led to performance degradation. Microstructural studies confirmed a significant change in the Ni-YSZ microstructure and the TPB length of operated samples was found to be two-thirds of the unoperated cermet. Knibbe et al. [98] also performed studies at high electrolysis current densities ($>-1 \text{ A cm}^{-2}$). They found that cell voltage degradation is predominately attributed to ohmic degradation and there is no direct relationship between polarization resistance degradation and current density/cell polarization. The degradation was also observed by an intergranular fracture degradation near the oxygen electrode/electrolyte interface. Across this grain boundary they found an increase in oxygen in the porous region. Similar findings were reported on microtubular SOECs [99]. They found that when operating at current densities of above -1.75 A cm^{-2} at 895 °C and 70% RH of steam, clear degradation was observed in the electrochemical data and this is confirmed by SEM micrographs (Fig. 11), EDS analysis and Raman spectroscopy. As with the results from Knibbe et al. [98], they detected voids at the grain boundaries of the YSZ in the region adjacent to the oxygen electrode, even generating large cracks in the electrolyte. The presence of excess oxygen near the oxygen electrode degraded regions is associated with the high p_{O_2} at the electrolyte–electrode interface, in concordance with Virkar's model [100], producing an irreversible degradation of the electrolyte due to YSZ electroreduction and, in some cases, the delamination of the oxygen electrode. Similar findings were also reported by Schefold et al. [101] using YSZ planar cells. They

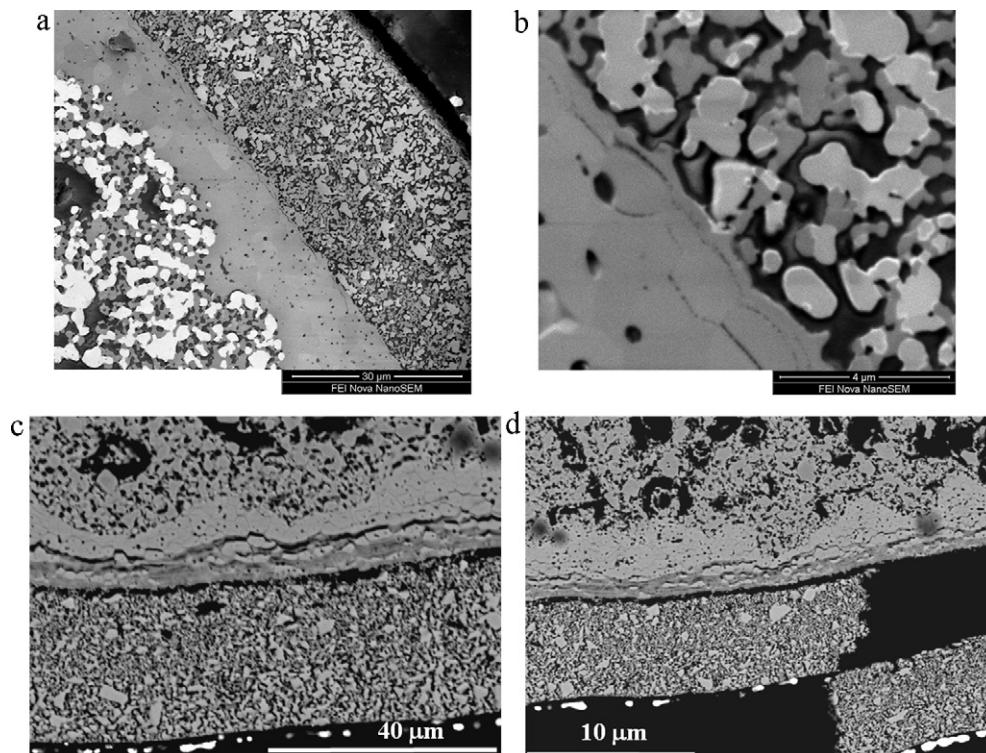


Fig. 11. SEM micrographs showing different stages of damage for the same cell (a) general view of the cell; (b) origin of the degradation at the YSZ grain boundaries; (c) cracking of the YSZ electrolyte and (d) delamination of the LSM-YSZ electrode, according to Ref. [99].

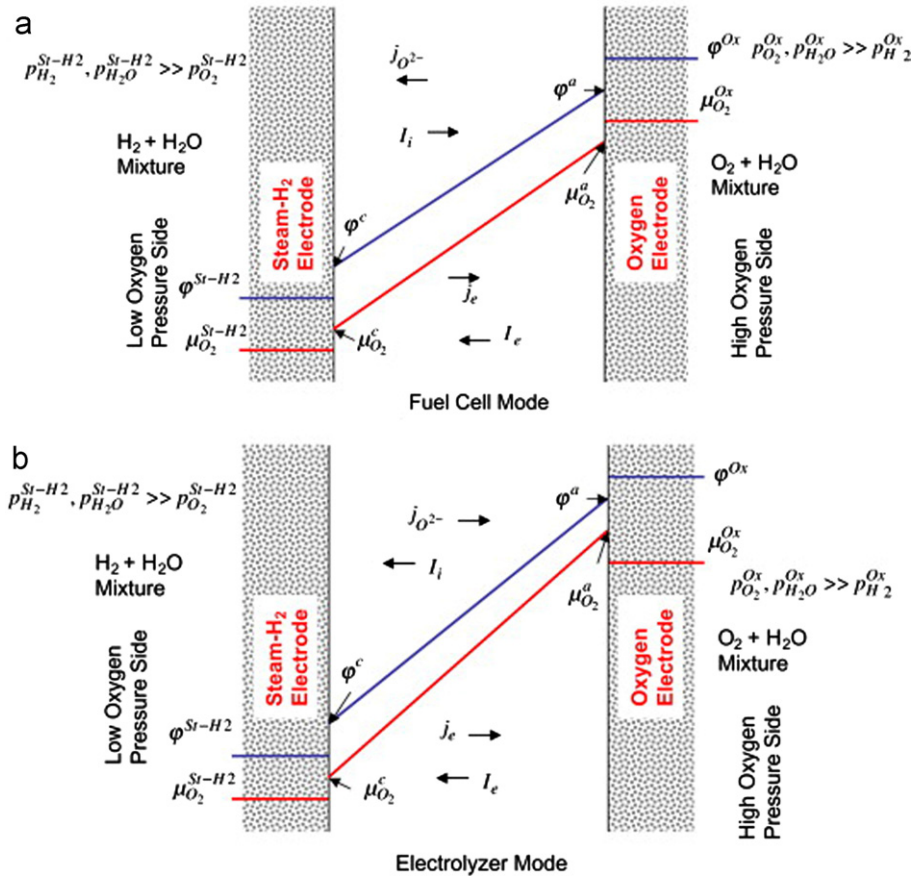


Fig. 12. (a) Schematic variations according to Ref. [100] of electric potential and oxygen chemical potential through the electrolyte in the fuel cell mode ('true' steady state). The directions of the particle fluxes are shown as well as the directions of ionic current and electronic current. (b) Schematic variations of electric potential and oxygen chemical potential through the electrolyte in the electrolyzer mode. Delamination along the electrolyte/anode (oxygen electrode) is likely in such a case. Elsevier permission.

observed that when operating at current densities which correspond to a steam-conversion rate above 100%, or when steam supply is interrupted under constant current, electronic conduction in the YSZ electrolyte takes place.

As previously mentioned, these findings were predicted by Virkar's model [100]. The model showed that electronic conduction in the electrolyte plays a crucial role in determining local oxygen chemical potential within the electrolyte. Under certain conditions, high pressures can develop in the electrolyte very near the oxygen electrode/electrolyte interface, leading to oxygen electrode delamination. This model also found that the higher the electronic conductivity of the electrolyte, the lower the tendency for high internal pressures to form. Preliminary calculations show that small changes in electronic conduction can cause changes of orders of magnitude in oxygen partial pressure, and thus, a small amount of electronic conduction through the electrolyte is beneficial for the material stability. Schematic variations of electric potential and oxygen chemical potential can be observed in Fig. 12.

In this respect, the recent findings on the Scandia and ceria-doped zirconia (10Sc1CeSZ) degradation under extreme SOEC conditions are also relevant [102]. This material presents an advantage compared to the standard YSZ. In this case, due to the presence of the Ce⁴⁺ dopant, which is reduced to Ce³⁺ during SOEC operation, it was possible to study the degradation monitoring the Ce⁴⁺ ↔ Ce³⁺ transition by spatially resolved vibrational and Ce³⁺ electronic micro-Raman spectroscopy and also by Er³⁺ luminescence spectroscopy. They observed that electrolyte reduction occurs near the Ni-YSZ electrode and then progresses along the thickness of the

electrolyte and in some cases is also associated with a phase change of the electrolyte from cubic to rhombohedral. They also observed that this degradation occurs when the cells are operated above 1.8 V.

To summarize, all these studies confirm that further microstructural improvements of the existing materials and/or the development of novel materials are required prior to commercialization of SOEC devices.

4. Modeling of solid oxide electrolysis cells and systems

Mathematical models are of great importance for the design of technological devices, especially if they are still under development, as in the case of SOECs. Prediction of the performance under different conditions is essential. A large number of works have been done in the last 5 years. In the present section, a short summary of these activities will be given. Additional information can be found in the following references [103–105]. Of great interest are the works of Udagawa et al. at Imperial College [106–108]. They developed an electrochemical model coupled to mass and energy balances to study the steady state behavior of a SOEC stack using conventional materials at different current densities and temperatures. They found that activation overpotentials produce irreversible losses while concentration overpotentials remained negligible. They also calculated an electrical consumption of around 3 kWh per m³ of hydrogen at 1023 K and a current density of -0.7 A cm^{-2} .

Ni et al. [109–111] also developed a model for SOEC using the Nernst and Butler–Volmer equations, Fick's model and Ohm's law and found that the model fits in well with the experimental

data available in the literature. Other thermodynamics and electrochemical models regarding hydrogen production using SOEC can be found in the literature [112–123].

5. Other applications using solid oxide electrolysis cells

Apart from hydrogen production, in very recent years SOFC cells have been proposed for a wide range of different applications [124]. An interesting approach was made by Martínez-Frias et al. [125]. They proposed a novel and highly efficient solid oxide natural gas-assisted steam electrolyser (NGASE), where natural gas reacts with the oxygen produced in the electrolysis, reducing the chemical potential across the electrolyser, thus minimizing electricity consumption. In this system, the oxygen produced during electrolysis could either be consumed in a partial or a total oxidation reaction with natural gas (Eqs. (9) and (10)):



Their analysis concluded that by incorporating a heat recovery system into the device, the efficiency will be around 70% with respect to primary energy. In this field, Wang et al. [126] studied Cu–CeO₂–YSZ and Pd–CeO₂–YSZ composites as the anode for NGASE and also for CO assisted steam electrolysis. They found that the Cu composite presents low catalytic activity when exposed to CO or CH₄. They also found that Pd composites have the highest catalytic activity, although the oxidation of CH₄ on the anode was significantly less than the theoretical value.

Pati et al. [127] also demonstrated that a solid oxide membrane (SOM) electrolyser could be used to produce hydrogen from steam using solid carbon reductant in liquid metal anode. They confirmed that the energy required for hydrogen production can be effectively lowered by feeding a solid carbon reductant into the liquid tin anode. The feasibility of hydrogen production from carbon and steam was also demonstrated by Lee et al. [128]. They used a YSZ cell with platinum electrodes, and the system was shown to produce spontaneous carbon-free hydrogen and cogeneration of electricity during galvanostatic operation.

As previously mentioned, the potential advantage of SOECs is their chemical flexibility, such as CO₂ electrolysis (Eq. (11)) [129] or, probably of greater interest, the co-electrolysis of steam and CO₂ to produce syngas (Eq. (12)). For example, renewable or nuclear energy could be used to produce the required heat and electricity for CO₂ and H₂O splitting.



Research into co-electrolysis is nowadays very active as well as promising, especially when combined with renewable or nuclear energy, as it could be used to recycle CO₂ into sustainable hydrocarbon fuels [130–139].

6. Summary

High temperature electrolysis using SOFC cells were presented as a promising alternative to the existing water electrolysis methods for hydrogen production. In addition, due to the chemical flexibility of those devices, it has been demonstrated that they could be used for the electrolysis of CO₂ to CO, and also for the co-electrolysis of H₂O/CO₂ to H₂/CO (syngas). In the present manuscript, current state in terms of electrolyte materials, fuel and oxygen electrodes, and material degradation issues has been reviewed in detail. This technology has huge potential although the understanding of the structure and electrochemistry of the materials is essential to future developments. In addition, development

of novel materials is required prior to commercialization of SOEC devices.

Acknowledgements

I would like to thank grant no. MAT2009-14324-C02-01 financed by the Spanish Government, and also the JA Eprogram (CSIC) for financial support.

References

- [1] H.F. Abbas, W. Daud, *Int. J. Hydrogen Energy* 35 (2010) 1160–1190.
- [2] M. Balat, *Int. J. Hydrogen Energy* 33 (2008) 4013–4029.
- [3] M. Balat, *Int. J. Hydrogen Energy* 34 (2009) 3589–3603.
- [4] Z.B. Chen, T.F. Jaramillo, T.G. Deutsch, A. Kleiman-Shwarstein, A.J. Forman, N. Gaillard, R. Garland, K. Takanabe, C. Heske, M. Sunkara, E.W. McFarland, K. Domen, E.L. Miller, J.A. Turner, H.N. Dinh, *J. Mater. Res.* 25 (2010) 3–16.
- [5] R. Elder, R. Allen, *Prog. Nucl. Energy* 51 (2009) 500–525.
- [6] P.C. Hallenbeck, D. Ghosh, *Trends Biotechnol.* 27 (2009) 287–297.
- [7] J.D. Holladay, J. Hu, D.L. King, Y. Wang, *Catal. Today* 139 (2009) 244–260.
- [8] Y. Kalinci, A. Hepbasli, I. Dincer, *Int. J. Hydrogen Energy* 34 (2009) 8799–8817.
- [9] R. Kothari, D. Buddhi, R.L. Sawhney, *Renew. Sust. Energy Rev.* 12 (2008) 553–563.
- [10] A. Kumar, D.D. Jones, M.A. Hanna, *Energies* 2 (2009) 556–581.
- [11] B.E. Logan, D. Call, S. Cheng, H.V.M. Hamelers, T. Sleutels, A.W. Jeremiasse, R.A. Rozendal, *Environ. Sci. Technol.* 42 (2008) 8630–8640.
- [12] M. Momirlan, T. Veziroglu, *Renew. Sust. Energy Rev.* 3 (1999) 219–231.
- [13] R.M. Navarro, M.C. Sanchez-Sanchez, M.C. Alvarez-Galvan, F. del Valle, J.L.G. Fierro, *Energy Environ. Sci.* 2 (2009) 35–54.
- [14] M. Ni, D.Y.C. Leung, M.K.H. Leung, *Int. J. Hydrogen Energy* 32 (2007) 3238–3247.
- [15] M. Ni, M.K.H. Leung, D.Y.C. Leung, K. Sumathy, *Renew. Sust. Energy Rev.* 11 (2007) 401–425.
- [16] J.W. Phair, S.P.S. Badwal, *Sci. Technol. Adv. Mater.* 7 (2006) 792–805.
- [17] I. Valdez-Vazquez, H.M. Poggi-Valardo, *Renew. Sust. Energy Rev.* 13 (2009) 1000–1013.
- [18] A. Yilanci, I. Dincer, H.K. Ozturk, *Progr. Energy Combust. Sci.* 35 (2009) 231–244.
- [19] K. Zeng, D.K. Zhang, *Progr. Energy Combust. Sci.* 36 (2010) 307–326.
- [20] W. Donitz, E. Erdle, *Int. J. Hydrogen Energy* 10 (1985) 291–295.
- [21] A.O. Isenberg, *Solid State Ionics* 3–4 (1981) 431–437.
- [22] W. Donitz, R. Streicher, *Chem. Ing. Tech.* 52 (1980) 436–438.
- [23] A. Hauch, S.D. Ebbesen, S.H. Jensen, M. Mogensen, *J. Mater. Chem.* 18 (2008) 2331–2340.
- [24] S.C. Singhal, K. Kendall (Eds.), *High Temperature SOFCs: Fundamentals, Design and Applications*, Elsevier, 2003.
- [25] S.J. Skinner, M.A. Laguna-Bercero, in: W. Duncan, R. Bruce, D. Walton, O'Hare (Eds.), *Advanced Inorganic Materials for Solid Oxide Fuel Cells in Energy Materials*, Wiley-VCH Verlag GmbH & Co. KGaA, Weinheim, 2011, pp. 33–94.
- [26] A.J. Jacobson, *Chem. Mater.* 22 (2010) 660–674.
- [27] A. Orera, P.R. Slater, *Chem. Mater.* 22 (2010) 675–690.
- [28] J.E. O'Brien, C.M. Stoots, J.S. Herring, J. Hartvigsen, *J. Fuel Cell Sci. Technol.* 3 (2006) 213–219.
- [29] M.A. Laguna-Bercero, S.J. Skinner, J.A. Kilner, *J. Power Source* 192 (2009) 126–131.
- [30] K. Eguchi, T. Hatagishi, H. Arai, *Solid State Ionics* 86–88 (1996) 1245–1249.
- [31] B. Zhu, I. Albinsson, C. Anderson, K. Borsand, M. Nilsson, B.-E. Mellander, *Electrochem. Commun.* 8 (2006) 495–498.
- [32] T. Ishihara, N. Jirathiwathanakul, H. Zhong, *Energy Environ. Sci.* 3 (2010) 665–672.
- [33] T. Ishihara, T. Kannou, *Solid State Ionics* 192 (2011) 642–644.
- [34] H. Uchida, N. Osada, M. Watanabe, *Electrochem. Solid State Lett.* 7 (2004) A500–A502.
- [35] O.A. Marina, L.R. Pederson, M.C. Williams, G.W. Coffey, K.D. Meinhardt, C.D. Nguyen, E.C. Thomsen, *J. Electrochem. Soc.* 154 (2007) B452–B459.
- [36] X. Yang, J.T.S. Irvine, *J. Mater. Chem.* 18 (2008) 2349–2354.
- [37] W. Wang, Y. Huang, S. Jung, J.M. Vohs, R.J. Gorte, *J. Electrochem. Soc.* 153 (2006) A2066–A2070.
- [38] F. Chauveau, J. Mougín, J.M. Bassat, F. Mauvy, J.C. Grenier, *J. Power Sources* 195 (2010) 744–749.
- [39] Q.A. Liu, C.H. Yang, X.H. Dong, F.L. Chen, *Int. J. Hydrogen Energy* 35 (2010) 10039–10044.
- [40] W. Suksamai, I. Metcalfe, *Solid State Ionics* 178 (2007) 627–634.
- [41] W. Donitz, G. Dietrich, E. Erdle, R. Streicher, *Int. J. Hydrogen Energy* 13 (1988) 283–287.
- [42] E. Erdle, W. Donitz, R. Schamm, A. Koch, *Int. J. Hydrogen Energy* 17 (1992) 817–819.
- [43] K.H. Quandt, R. Streicher, *Int. J. Hydrogen Energy* 11 (1986) 309–315.
- [44] N.J. Maskalick, *Int. J. Hydrogen Energy* 11 (1986) 563–570.
- [45] A. Momma, T. Kato, Y. Kaga, S. Nagata, *J. Ceram. Soc. Jpn.* 105 (1997) 369–373.
- [46] <http://www.relhy.eu/>.
- [47] J.P. Ouweltjes, M.M.A. van Tuel, F.P.F. van Berkel, G. Rietveld, *ECS Trans.* 7 (2007) 933–940.

- [48] A. Brisse, J. Schefold, M. Zahid, *Int. J. Hydrogen Energy* 33 (2008) 5375–5382.
- [49] A. Hauch, J.S.H. Jensen, S. Ramousse, M. Mogensen, *J. Electrochem. Soc.* 153 (2006) A1741–A1747.
- [50] P. Kim-Lohsoontorn, N. Laosiripojana, J. Bae, *Curr. Appl. Phys.* 11 (2011) S223–S228.
- [51] S. Elangovan, J.J. Hartvigsen, *Int. J. Appl. Ceram. Technol.* 4 (2007) 109–118.
- [52] T. Ishihara, T. Kanno, *ISIJ Int.* 50 (2010) 1291–1295.
- [53] T. Schober, *Solid State Ionics* 139 (2001) 95–104.
- [54] N. Bonanos, B. Ellis, M.N. Mahmood, *Solid State Ionics* 44 (1991) 305–311.
- [55] H. Iwahara, T. Esaka, H. Uchida, T. Yamauchi, K. Ogaki, *Solid State Ionics* 18–19 (1986) 1003–1007.
- [56] W. Coors, *J. Power Sources* 118 (2003) 150–156.
- [57] P. Stuart, Ph.D. Thesis, Imperial College London, 2009.
- [58] H. Iwahara, T. Esaka, H. Uchida, N. Maeda, *Solid State Ionics* 3–4 (1981) 359–363.
- [59] H. Matsumoto, M. Okubo, S. Hamajima, K. Katahira, H. Iwahara, *Solid State Ionics* 152–153 (2002) 715–720.
- [60] T. Kobayashi, K. Abe, Y. Ukyo, H. Iwahara, *Solid State Ionics* 154–155 (2002) 699–705.
- [61] J.T.S. Irvine, A. Kruth, C.D. Savaniu, S. Tao, “Steam electrolysis” World Intellectual Property Organisation, p. WO 2005/093130 (2005).
- [62] P.A. Stuart, T. Unno, J.A. Kilner, S.J. Skinner, *Solid State Ionics* 179 (2008) 1120–1124.
- [63] T. Sakai, S. Matsushita, H. Matsumoto, S. Okada, S. Hashimoto, T. Ishihara, *Int. J. Hydrogen Energy* 34 (2009) 56–63.
- [64] F. He, D. Song, R.R. Peng, G.Y. Meng, S.F. Yang, *J. Power Sources* 195 (2010) 3359–3364.
- [65] R. Hino, Y. Miyamoto, *J. Atom. Energy Soc. Jpn.* 37 (1995) 1042–1049.
- [66] R. Hino, K. Haga, H. Aita, K. Sekita, *Nucl. Eng. Des.* 233 (2004) 363–375.
- [67] G. Schiller, A. ANsar, M. Lang, O. Patz, *J. Appl. Electrochem.* 39 (2009) 293–301.
- [68] K. Kendall, *Int. J. Appl. Ceram. Technol.* 7 (2010) 1–9.
- [69] K.V. Galloway, N.M. Sammes, *J. Electrochem. Soc.* 156 (2009) B526–B531.
- [70] T. Suzuki, Z. Hasan, Y. Funahashi, T. Yamaguchi, Y. Fujishiro, M. Awano, *Science* 325 (2009) 852–855.
- [71] S. Hashimoto, Y. Liu, M. Mori, Y. Funahashi, Y. Fujishiro, *Int. J. Hydrogen Energy* 34 (2009) 1159–1165.
- [72] M.A. Laguna-Bercero, R. Campana, A. Larrea, J.A. Kilner, V.M. Orera, *J. Electrochem. Soc.* 157 (2010) B852–B855.
- [73] M.A. Laguna-Bercero, R. Campana, A. Larrea, J.A. Kilner, V.M. Orera, *Fuel Cells* 11 (2011) 116–123.
- [74] A. Hauch, S.D. Ebbesen, S.H. Jensen, M. Mogensen, *J. Electrochem. Soc.* 155 (2008) B1184–B1193.
- [75] A. Hauch, S.H. Jensen, J.B. Bilde-Sorensen, M. Mogensen, *J. Electrochem. Soc.* 154 (2007) A619–A626.
- [76] T. Matsui, R. Kishida, J.Y. Kim, H. Muroyama, K. Eguchi, *J. Electrochem. Soc.* 157 (2010) B776–B781.
- [77] N. Osada, H. Uchida, M. Watanabe, *J. Electrochem. Soc.* 153 (2006) A816–A820.
- [78] V.I. Sharma, B. Yildiz, *J. Electrochem. Soc.* 157 (2010) B441.
- [79] M.S. Sohal, J.E. O'Brien, C.M. Stoots, J.S. Herring, J. Hartvigsen, D. Larsen, S. Elangovan, J.D. Carter, V.I. Sharma, B. Yildiz, Report No. INL/EXT-09-16004, Report to the U.S. Department of Energy by Idaho National Laboratory, 2009.
- [80] M. Liang, B. Yu, M. Wen, J. Chen, J. Xu, Y. Zhai, *J. Power Sources* 190 (2009) 341–345.
- [81] W. Wan, S.P. Jiang, *Solid State Ionics* 177 (2006) 1361–1369.
- [82] M. Backhaus-Ricoult, K. Adib, T.St. Clair, B. Luerssers, L. Gregoratti, A. Barinov, *Solid State Ionics* 179 (2008) 891.
- [83] C. Yang, A. Coffin, F. Chen, *Int. J. Hydrogen Energy* 35 (2010) 3221–3226.
- [84] X.J. Chen, S.H. Chan, K.A. Khor, *Electrochem. Solid-State Lett.* 7 (2004) A144–A147.
- [85] K. Chen, N. Ai, S.P. Jiang, *J. Electrochem. Soc.* 157 (2010) P89–P94.
- [86] R.J. Gorte, J.M. Vohs, *J. Catal.* 216 (2003) 477.
- [87] S.P. Jiang, S. Zhang, Y.D. Zhen, A.P. Koh, *Electrochem. Solid-State Lett.* 7 (2004) A282.
- [88] J. Kong, Y. Zhang, C. Deng, J. Xu, *J. Power Sources* 186 (2009) 485–489.
- [89] M.A. Laguna-Bercero, J.A. Kilner, S.J. Skinner, *Chem. Mater.* 22 (2010) 1134–1141.
- [90] M.A. Laguna-Bercero, J.A. Kilner, S.J. Skinner, *Solid State Ionics* 192 (2011) 501–504.
- [91] Y. Bo, Z. Wenquiang, C. Jin, *Int. J. Hydrogen Energy* 33 (2008) 6873–6877.
- [92] P. Kim-Lohsoontorn, D.J.L. Brett, N. Laosiripojana, Y.-M. Kim, J.-M. Bae, *Int. J. Hydrogen Energy* 35 (2010) 3958–3966.
- [93] Y. Tao, H. Nishino, S. Ashidate, H. Kokubo, M. Watanabe, H. Uchida, *Electrochim. Acta* 54 (2009) 2209–2315.
- [94] F. Chauveau, J. Mouglin, F. Mauvy, J.-M. Bassat, J.-C. Grenier, *Int. J. Hydrogen Energy* 36 (2011) 7785–7790.
- [95] M.A. Laguna-Bercero, N. Kinadjian, R. Sayers, H. El Shinawi, C. Greaves, S.J. Skinner, *Fuel Cells* 11 (2011) 102–107.
- [96] M.S. Sohal, J.E. O'Brien, C.M. Stoots, V.I. Sharma, B. Yildiz, A. Virkar, *Proceedings of the ASME Fuel Cell*, 2010, pp. 1–11.
- [97] J.R. Mawdsley, J.D. Carter, A.J. Kropf, B. Yildiz, V.A. Maroni, *Int. J. Hydrogen Energy* 34 (2009) 4198–4207.
- [98] R. Knibbe, M.L. Traulsen, A. Hauch, S.D. Ebbesen, M. Mogensen, *J. Electrochem. Soc.* 157 (2010) B1209–B1217.
- [99] M.A. Laguna-Bercero, R. Campana, A. Larrea, J.A. Kilner, V.M. Orera, *J. Power Sources* 196 (2011) 8942–8947.
- [100] A.V. Virkar, *Int. J. Hydrogen Energy* 35 (2010) 9527–9533.
- [101] J. Schefold, A. Brisse, M. Zahid, *J. Electrochem. Soc.* 156 (2009) B897.
- [102] M.A. Laguna-Bercero, V.M. Orera, *Int. J. Hydrogen Energy* 36 (2011) 13051–13058.
- [103] M. Ni, M.K.H. Leung, D.Y.C. Leung, *Int. J. Hydrogen Energy* 33 (2008) 2337–2354.
- [104] C. Athanassiou, G. Pekridis, N. Kakkidis, K. Kalimeri, S. Vartzoka, G. Marnellos, *Int. J. Hydrogen Energy* 32 (2007) 38–54.
- [105] B. Yu, W.Q. Zhang, J. Chen, J.M. Xu, *Sci. China B* 51 (2008) 289–304.
- [106] J. Udagawa, P. Aguiar, N.P. Brandon, *J. Power Sources* 166 (2007) 127–136.
- [107] J. Udagawa, P. Aguiar, N.P. Brandon, *J. Power Sources* 170 (2008) 46–55.
- [108] J. Udagawa, P. Aguiar, N.P. Brandon, *J. Power Sources* 170 (2008) 354–364.
- [109] M. Ni, M.K.H. Leung, D.Y.C. Leung, *Chem. Eng. Technol.* 29 (2006) 636–642.
- [110] M. Ni, M.K.H. Leung, D.Y.C. Leung, *Electrochim. Acta* 52 (2007) 6707–6718.
- [111] M. Ni, *Int. J. Hydrogen Energy* 34 (2009) 7795–7806.
- [112] Y. Shin, W. Park, J. Chang, J. Park, *Int. J. Hydrogen Energy* 32 (2007) 1486–1491.
- [113] S. Fujiwara, S. Kasai, H. Yamauchi, K. Yamada, S. Makino, K. Matsunaga, M. Yoshino, T. Kameda, T. Ogawa, S. Momma, E. Hoashi, *Prog. Nucl. Energy* 50 (2008) 422–426.
- [114] S. Gopalan, M. Mosleh, J.J. Hartvigsen, R.D. McConnell, *J. Power Sources* 185 (2008) 1328–1333.
- [115] L. Mingyi, Y. Bo, X. Jingming, C. Jing, *J. Power Sources* 177 (2008) 493–499.
- [116] P. Iora, P. Chiesa, *J. Power Sources* 190 (2009) 408–419.
- [117] D. Grondin, J. Deseure, A. Brisse, M. Zahid, P. Ozil, *J. Appl. Electrochem.* 40 (2010) 933–941.
- [118] X. Jin, X. Xue, *Int. J. Hydrogen Energy* 35 (2010) 7321–7328.
- [119] P. Iora, M.A.A. Taher, P. Chiesa, N.P. Brandon, *Int. J. Hydrogen Energy* 35 (2010) 12680–12687.
- [120] N. Perdikaris, K.D. Panopoulos, Ph. Hofmann, S. Spyrikis, E. Kakaras, *Int. J. Hydrogen Energy* 35 (2010) 2446–2456.
- [121] Q. Cai, E. Luna-Ortiz, C.S. Adjiman, N.P. Brandon, *Fuel Cells* 10 (2010) 1114–1128.
- [122] J. Laurencin, D. Kane, G. Delette, J. Deseure, F. Lefebvre-Joud, *J. Power Sources* 196 (2011) 2080–2093.
- [123] J.E. O'Brien, M.G. McKellar, E.A. Harvego, C.M. Stoots, *Int. J. Hydrogen Energy* 35 (2010) 4808–4819.
- [124] C. Graves, S.D. Ebbesen, M. Mogensen, K.S. Lackner, *Renew. Sust. Energy Rev.* 15 (2011) 1–23.
- [125] J. Martinez-Frias, A.-Q. Pham, S.M. Aceves, *Int. J. Hydrogen Energy* 28 (2003) 483–490.
- [126] W. Wang, J.M. Vohs, R.J. Gorte, *Top. Catal.* 46 (2007) 380–385.
- [127] S. Pati, K.J. Yoon, S. Gopalan, U.B. Pal, *J. Electrochem. Soc.* 156 (2009) B1067–B1077.
- [128] A.C. Lee, R.E. Mitchell, T.M. Gür, *Solid State Ionics* 192 (2011) 607–610.
- [129] S.D. Ebbesen, M. Mogensen, *J. Power Sources* 193 (2009) 349–358.
- [130] G. Tao, K.R. Sridhar, C.L. Chan, *Solid State Ionics* 175 (2004) 615–619.
- [131] C.-G. Fan, T. Iida, K. Murakami, T. Matsui, R. Kikuchi, K. Eguchi, *J. Fuel Cell Sci. Technol.* 5 (2008) 031202–31211.
- [132] J. Hartvigsen, S. Elangovan, L. Frost, A. Nickens, C. Stoots, J. O'Brien, J.S. Herring, *ECS Trans.* 12 (2008) 625–637.
- [133] C. Graves, S.D. Ebbesen, M. Mogensen, *Solid State Ionics* 192 (2011) 398–403.
- [134] Z. Zhang, W. Kobsiriphat, J.R. Wilson, M. Pillai, I. Kim, S.A. Barnett, *Energy Fuels* 23 (2009) 3089–3096.
- [135] C. Stoots, J. O'Brien, J. Hartvigsen, *Int. J. Hydrogen Energy* 34 (2009) 4208–4215.
- [136] M. Ni, *Chem. Eng. J.* 164 (2010) 246–254.
- [137] C. Stoots, J. O'Brien, J.S. Herring, J. Hartvigsen, *J. Fuel Cell Sci. Technol.* 6 (2009) 011014-1–011014-12.
- [138] Q.X. Fu, C. Malibat, M. Zahid, A. Brisse, L. Gautier, *Energy Environ. Sci.* 3 (2010) 1382–1397.
- [139] S.H. Jensen, X. Sun, S.D. Ebbesen, R. Knibbe, M. Mogensen, *Int. J. Hydrogen Energy* 35 (2010) 9544–9549.
- [140] C.M. Stoots, J.E. O'Brien, K.G. Condie, J.J. Hartvigsen, *Int. J. Hydrogen Energy* 35 (2010) 4861–4870.